

**Development of a Compact Optical Communications Terminal for the  
PULSE-A CubeSat**

Sofia Mansilla, Seth Knights, Natalie Orrantia, Maya McDaniel, Daniel Lee, Oliver Shoemaker, Aidan Etterer, Aishani Mohan, Chris Wong, Juan Ignacio Prieto Asbun, Robert Pitu, Logan Hansler, Annie Shuford, Eliana Schiller, Kira Chin, Graydon Schulze-Kalt, Danielle Zumi Riekse, Mira Singh, Alexandra Yao, Vicky Bardon Soto, Natalie Sauer, Vidya Suri, Tian Zhong.

The University of Chicago  
Eckhardt, 5640 S Ellis Ave, Chicago, IL 60637; 872-335-6826  
smansilla@uchicago.edu  
mansillasofia83@gmail.com  
+1 (786) 461-7752

**ABSTRACT**

The Polarization-modUlated Laser Satellite Experiment (PULSE-A) at the University of Chicago aims to demonstrate the feasibility of circular polarization shift keyed (CPolSK) satellite-to-ground laser communication links. The project aims to advance high-speed optical satellite-to-ground communications as an alternative to the traditionally used radio frequencies. PULSE-A thus requires the development of a compact, low-loss optical communications terminal capable of emitting collimated and high-power circularly polarized light modulated at high frequencies. Here we present a design for an optical communications terminal capable of achieving output powers of up to 230 mW at modulation frequencies from 1 to 10 MHz with a maximum coupled pointing error of less than 1 mrad. The optical communications terminal consists of two primary interrelated paths: (1) a collection path to gather, filter, and detect a 1064 nm beacon laser from the optical ground station and (2) a transmission path to emit, modulate, and amplify an outgoing 1550 nm transmission beam. During a pass, body-pointing aims the satellite's optical aperture towards the ground station. The collection path gathers and focuses beacon light via a Keplerian beam condenser, blocks irrelevant wavelengths with a filter stack, and focuses the remaining light onto a quadrant photodiode detector. This detector supplies feedback to a fine steering mirror, which performs slight adjustments to center the beacon on the detector. The transmission path begins with two linear, orthogonally polarized seed lasers which encode data by alternately turning ON and OFF at a frequency of 1–10 MHz. This signal is then amplified to 250 mW using a random polarization erbium-doped fiber amplifier (EDFA) and passed through a quarter wave plate to convert the signal to circular polarization states. The collection and transmission paths are combined via an 1180 nm-cutoff shortpass dichroic mirror into a single optical path as they approach the fine steering mirror (FSM). This FSM- and detector-based feedback loop, pioneered by MIT's CLICK-A and DLR's OSIRIS4CubeSat missions for the CubeSat form factor, allows for a simple fine-pointing scheme where when the received beacon is aimed at the center of the quadrant photodiode in the collection path, the transmission beam and the ground station beacon are co-boresight. A 638 nm beacon subassembly with a significantly wider divergence assists the optical ground station with tracking the satellite's location throughout transmission. Structurally, the use of fiber-optic connections and a baffling system will mitigate stray light and reduce the overall volume of the communications terminal. Current development includes optical component selection, simulation in Zemax OpticStudio, and testing of fiber-optic systems and the quadrant photodiode on the bench. The optical terminal design, along with its driving requirements, simulations and testing, and our approaches to various hurdles in creating a small form factor CPolSK optical communications terminal are presented here.

## 1. Introduction

In recent years, the use of commercial off-the-shelf (COTS) hardware, along with the ease of deployment and scalability of small satellites, particularly CubeSats, has made them an increasingly popular platform for scientific and commercial applications ranging from Earth observation to communication services. Motivated by these recent advancements in the realm of space-to-ground optical communications, the Polarization modUlated Laser Satellite Experiment (PULSE-A) is currently under development at the University of Chicago. PULSE-A is a 3U CubeSat-scale space-to-ground optical communications satellite that aims to advance laser-communication technology. It shall achieve data rates up to 10 Mbps—roughly an order of magnitude higher than typical CubeSat RF links—while demonstrating the feasibility of free-space circular polarization shift-keying (CPolSK) and delivering a Payload optimized for 3U CubeSat size and weight constraints.

This paper presents the design of the PULSE-A optical Payload: a small form-factor, monostatic optical communications terminal designed for circular polarization-based modulation schemes. This paper is organized around four main sections: (1) An overview of the mission and its pointing, acquisition, and tracking (PAT) sequence, along with the driving system requirements for data transmission and pointing accuracy; (2) A comprehensive description of the Payload and its six assemblies, including descriptions of guiding component studies; (3) a summary of ongoing laboratory experiment results with a particular emphasis on maintaining polarization integrity; and (4) a detailed review of the payload’s mechanical architecture, including enclosure materials and optomechanical design.

## 2. Concept of Operations

An overview of PULSE-A’s concept of operations is included in Figure 1. After launch, deployment, and initial setup, the satellite will be able to begin Payload operations. This is split into three major phases, the first being beacon acquisition, followed by the transition to closed-loop tracking and lastly, data transmission. The current expectation is for mission operations to last approximately one year, with launch occurring no earlier than Q1 2027 and Payload operations occurring throughout the duration of summer and early fall that year, to help maximize favorable weather conditions in the greater Chicago area where the Optical Ground Sta-

tion (OGS) will be based.

### 2.1. Pointing, Acquisition, and Tracking

Similar to other CubeSat lasercom missions, the PULSE-A Payload is not gimballed and pointing is enabled via a combination of the spacecraft’s bus and internal pointing mechanisms. To meet the strict pointing requirements necessary for optical communication, the Payload itself uses a beacon-based fine pointing architecture. The primary goal of this fine pointing mechanism is to align the outgoing transmission laser with the incoming beacon laser transmitted from the OGS, such that the transmission beam can be pointed with greater precision than with the spacecraft’s Attitude Determination and Control System (ADCS) alone, which is expected to achieve approximately  $\pm 1.00^\circ 3\sigma$  accuracy. A beacon laser on the Payload, which is not affected by the steering mechanism, provides confirmation to the OGS that the spacecraft’s body pointing is within the expected range. This high-precision alignment of both payload and ground-station optical axes, with sub-milliradian precision, is established before data transmission as part of the pointing, acquisition, and tracking (PAT) sequence.

Assuming the time and environmental factors of an individual pass prove it acceptable for attempting an optical link, both the spacecraft and OGS will begin blindly pointing at the expected location of the other. That is, the Optical Ground Station (OGS) initially directs its telescope toward the satellite’s predicted position using orbital and GPS data, with the payload commanding the satellite’s ADCS to do the same for the OGS. Acquisition begins when the OGS detects the Payload beacon using its tracking camera. After detecting the Payload beacon laser with its tracking camera, the system continuously monitors the position of the beacon relative to the camera center. If the beacon drifts from the optimal position, the OGS issues precise adjustment commands to the telescope mount, re-centering the beacon within the field of view. This feedback-controlled pointing ensures that the transmission laser remains precisely aligned, while also verifying that the spacecraft’s body pointing is maintained within the expected range established by the ADCS.

Once the telescope aligns itself with the Payload beacon, the OGS emits its own beacon. The Payload then detects the OGS beacon and proceeds to initiate tracking, forming a feedback loop to align its beam path with that of the ground beacon. This ensures that data can be transmitted in a co-

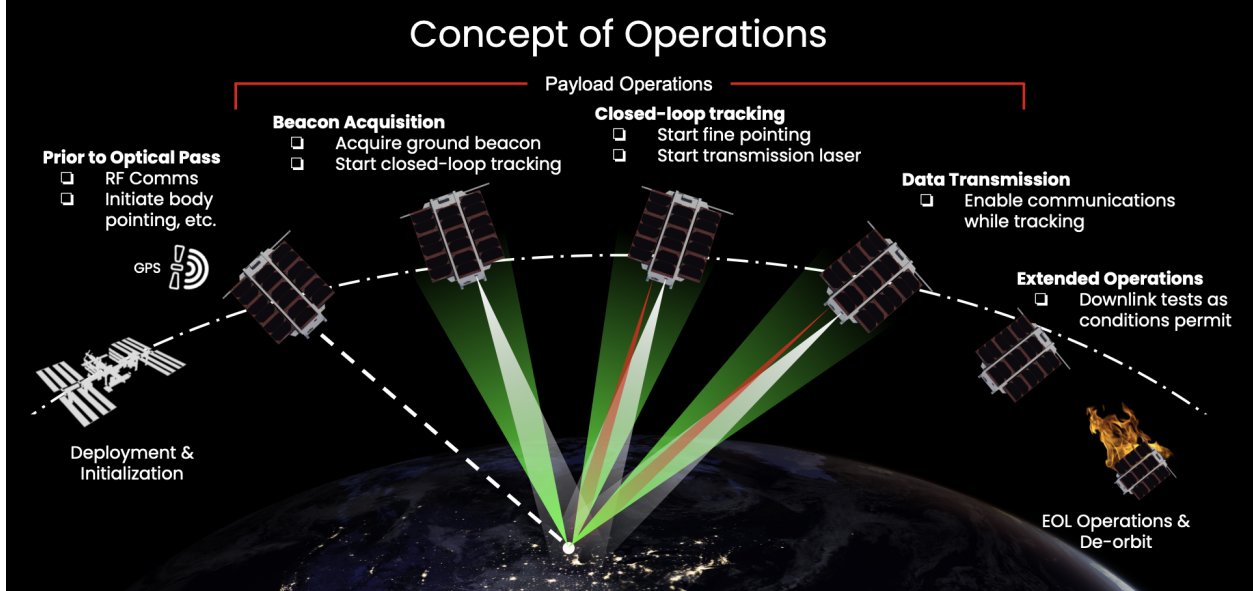


Figure 1: Diagram of PULSE-A mission proposed operations, indicating all stages of mission life. The diagram begins with deployment and ends with de-orbit.

boresighted configuration. Once acquisition is complete, the spacecraft will proceed with data transmission.

### 3. Payload General Design Overview

Designed to maintain fine pointing and deliver polarization-encoded optical data from space to ground, PULSE-A’s scientific payload integrates acquisition, alignment, amplification, and modulation into a compact optical communications terminal suitable for CubeSat-class missions. The terminal is divided into six sub-assemblies: **Beacon**, **Telescope**, **Detection**, **Steering**, **Transmission**, and **Injection**.

The Beacon sub-assembly transmits a stable, visible reference beam for the OGS tracking camera. The Telescope sub-assembly collects the incoming OGS beacon and delivers it to the Detection and Steering assemblies. The Detection sub-assembly measures the beacon’s position and sends error signals to the Steering sub-assembly, where a fast steering mirror (FSM) provides co-boresight alignment of the incoming beacon and outgoing transmission beams for fine pointing control. Finally, the Transmission and Injection sub-assemblies prepare the data-modulated, circularly polarized 1550 nm beam by amplifying it via the EDFA, collimating it, and encoding at 1-10 MHz, before combining it with the aligned beacon path for downlink.

#### 3.1. Driving Requirements

PULSE-A’s optical terminal requirements are comparable to those of other LEO laser-comm missions. PULSE-A must first ensure reliable ground acquisition via a 638 nm beacon, expected to diverge around 1–2 mrad and emit 200 mW. The system should also maintain a sub-milliradian pointing stability ( $\leq 0.2\text{mrad}$ ) to ensure sufficient alignment for the OGS detection of the encoded beam.

Table 1: PULSE-A Payload Driving Requirements and Reference Missions

Main Function	Subcategory	Requirement / Target Value	Our Expected Value	Reference and Explanation
Pointing	Beacon (downlink) Divergence	$\leq 6 \text{ dB of loss from satellite body mispointing}$	7.3 mag	• NICT SOTA: 2.0 mrad full-angle divergence
Pointing	Beacon (downlink) Power	$\geq 200 \text{ mW}$	200 mW	CLICK-A: designed $\geq 1 \text{ mW}$ received from $\sim 200 \text{ mW}$ tx
Pointing	Fine-Pointing Accuracy	$\leq 200 \text{ }\mu\text{rad RMS pointing error, to close link budget}$	$\leq 200 \text{ }\mu\text{rad by design, to be confirmed with ongoing testing}$	• CLICK-A: 136.9 $\mu\text{rad RMS}$ • TBIRD: 10 $\mu\text{rad RMS} @ 10 \text{ Hz}$
Data Transmission	Data-beam Speed	1-10 Mbps	1 Kbps -10 Mbps	• CLICK-A: 10 Mbps • O4C: up to 100 Mbps
Data Transmission	Data-beam Power	250 mW at EDFA output, to close link budget	250-300 mW via EDFA	• CLICK-A: • O4C: 100 mW EDFA
Data Transmission	Data-beam Divergence	0.83 mrad, to close link budget	0.92 mrad, based on COTS component	• CLICK-A: 1.3 mrad FWHM • O4C: 0.193 mrad

For the data channel, dual 1550 nm seed lasers

are polarization-modulated at 1–10 MHz, amplified up to  $\geq 250\text{mW}$ , and converted to circular polarization; ongoing bench tests will verify the maximum allowed degree of ellipticity for CPolSK to be decoded on the ground. Table 1 summarizes these system requirements alongside past mission examples [6][8].

### 3.2. Link Budgeting

Link budget analysis estimates the received average power by accounting for all gains and losses on the path between the transmitter and receiver. This accounting gives a final, received signal-to-noise ratio (SNR), which is a baseline for the effectiveness of continuous tracking and error rates of data decoding when relevant. [4] For the mission, a minimum worst-case link margin (SNR) of 6 dB was settled upon. When designing the Payload, we aimed to maximize the SNR on the ground for both the Payload beacon and downlink transmission laser; the primary considerations for this were wavelength, output power, and beam divergence. Table 2 lists the major considerations for the Payload’s transmission laser link budget.

The 1550 nm wavelength of the downlink beam was selected primarily due to its common use in telecommunications and prior success in a number of space-based optical communication missions. Thus, there is a broad array of COTS optical components made for operating in and around the 1550 nm band. Another major reason for using 1550 nm is its high atmospheric transmittance, which allows for less atmospheric attenuation and better overall link margin, shown explicitly in Figure 2.

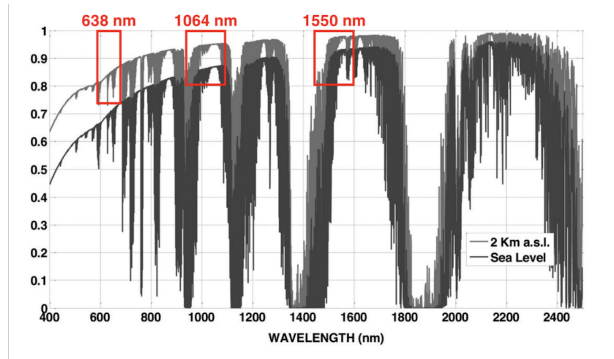


**Figure 2:** A plot of atmospheric transmittance for various wavelengths ranging from 400 nm to 2400 nm, adapted from Hemmati 2021 [3]. Red boxes highlight transmittance rates for the wavelengths selected for the PULSE-A mission.

**Table 2: Simplified Transmission Link Budget**

Parameter	Design Value
<i>Variables</i>	
Wavelength, m	1.55E-06
Distance, m	9.00E+05
Transmitter $\frac{1}{e^2}$ divergence, rad	9.20E-04
Receiver diameter, m	2.79E-01
Receiver NEP, W/ $\sqrt{\text{Hz}}$	1.30E-13
Data rate, bps	1.00E+06
Receiver sample rate, Hz	4.00E+06
Receiver noise power, dBm	-65.85
Receiver external noise, dBm	-63.01
<i>Transmitter</i>	
Laser output power, dBm	6.00
EOM insertion loss, dB	-3.00
EDFA gain, dB	21.00
Fiber connection loss, dB	-3.15
Optical antenna gain, dB	75.78
Optical system loss, dB	-1.50
Pointing loss, dB	-3.50
<i>Path</i>	
Space loss, dB	-257.26
Atmospheric attenuation, dB	-1.20
Scintillation loss, dB	-2.00
<i>Receiver</i>	
Telescope gain, dB	115.06
Telescope optical loss, dB	-2.17
Fiber coupling loss, dB	-1.00
<i>Summary</i>	
Received power, dBm	-56.94
Received SNR, dB	6.07

Alongside wavelength selection, determining the transmission beam divergence angle constitutes a fundamental link budget parameter that drives payload design choices. While a smaller divergence angle leads to better optical gain and thus a higher overall on-axis power, a narrower beam also leads to increasing off-axis losses. The optimal divergence angle balances on-axis power against expected pointing errors and allowable loss. By fixing the budgeted, worst-case pointing loss at a maximum of 3.5 dB, we find that 0.83 mrad divergence provides well over  $\pm 0.25$  mrad of mispointing margin before the 3.5 dB loss threshold is crossed. In the given budget, a 0.92 mrad full-angle divergence is assumed based on commercial component specifications.

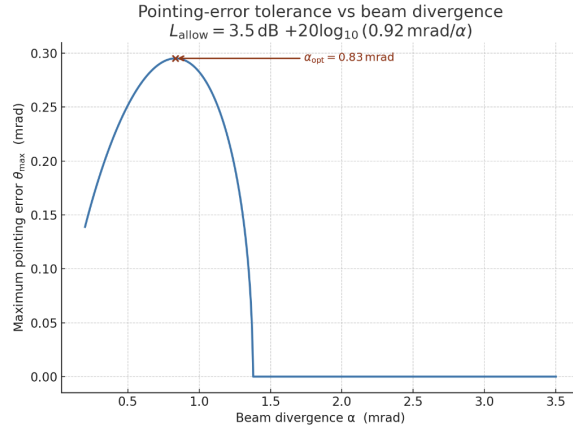


**Figure 3: A plot of maximum pointing angle of error as a function of collimator beam divergence angle, given a loss budget of 3.5 dB, and considering the loss to antenna gain caused by an increased divergence angle (present in the correction term on  $L_{\text{allow}}$ )**

For beacon power and divergence constraints, similar link budgeting can be done. For the OGS beacon, the power estimated at the receiving QPD is -58 dB, which is likely viable but requires further testing, especially with respect to atmospheric effects. Since the OGS beacon remains on the ground and thus has fewer constraints on power and divergence, testing will be used to optimize the system. Most notably, the team is currently exploring options for both modulating the uplink beam, such that the SNR at the QPD can be increased via band pass filtering, and using multiple apertures, to reduce the loss from scintillation effects (i.e. beam wander, which are much greater when traveling from ground to space). [3]

#### 4. Payload Detailed Design Overview

The following sections discuss the design and component selection process of each Payload subassembly, addressing key challenges of beam quality, polarization fidelity, and CubeSat-scale integration.

##### 4.1. Telescope Assembly

The Telescope assembly collects the incoming OGS beacon, which arrives as a collimated beam, and reduces its diameter through a  $4\times$  demagnification system. The Telescope assembly is composed of two plano-convex lenses, with focal lengths of 60 mm and 40 mm respectively, to ensure the beam fits within the fine steering mirror's 6.4 mm active area while preserving sufficient angular sensitivity for fine pointing. The first lens serves to converge the collimated beacon, while the second further focuses the beam to achieve the acquired four-times reduction. This optical compression is critical for maintaining the fine steering mirror's field of view without vignetting.

In a power-constrained laser communications system, maximizing the received power on the ground, and thus minimizing the transmission beam's mispointing, is key to maintaining link margin and therefore ensuring effective data transmission. With an expected full-angle output divergence on the order of 1 mrad, the power loss from one degree of mispointing would easily make the link nearly impossible to close. Therefore, the Payload is designed to provide fine-steering capabilities beyond that given by the spacecraft's COTS ADCS. Driven by the requirement that mispointing loss must be no less than 3.5 dB for the given output divergence, the steering mechanism must therefore augment the ADCS  $1.00^\circ 3\sigma$  body pointing such that the overall pointing error is less than 0.2 mrad. The PULSE-A payload does so with the use of a fairly standard, closed-loop feedback mechanism between the quadrant photodiode (QPD) and fine steering mirror (FSM), which is capable of detecting and correcting based on the OGS beacon's angle of arrival.

#### 4.2. Detector and Steering Assemblies

Since both the incoming and outgoing signals are aligned along the same optical path through the telescope assembly and off of the FSM, steering the received OGS beacon signal to the center of the QPD is equivalent to steering the transmitted signal back towards the angle of arrival. Thus, a much greater pointing accuracy can be achieved.

More specifically, the outgoing 1550 nm transmission beam is combined with the incoming 1064 nm OGS beacon via a short-pass dichroic mirror (1180 nm cutoff). The transmission beam is reflected on to the FSM and proceeds out through the telescope assembly and down to Earth. The incoming OGS beacon beam instead passes through the dichroic, and the remaining optical noise is then removed using a 1064 nm bandpass and a 1200 nm longpass filter, the second of which is included to provide better rejection of 1550 nm back-reflected transmission light. The beacon light is then focused by a plano-convex lens of 9mm focal length onto the InGaAs QPD.

## PULSE-A Optical Payload Diagram

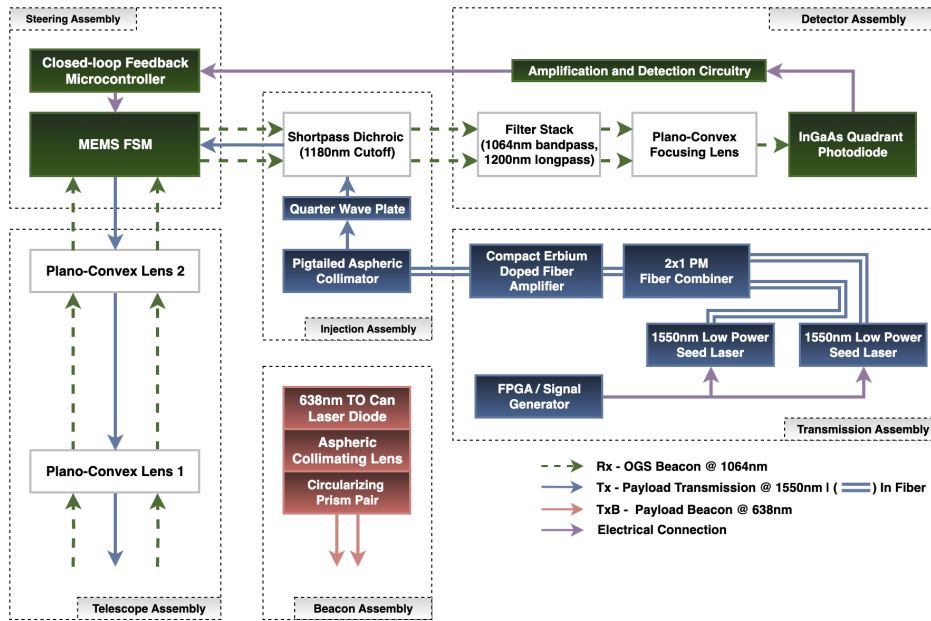


Figure 4: Diagram of Payload terminal layout, demonstrating beam path of transmission and beacon lasers. All Payload assemblies are labelled.

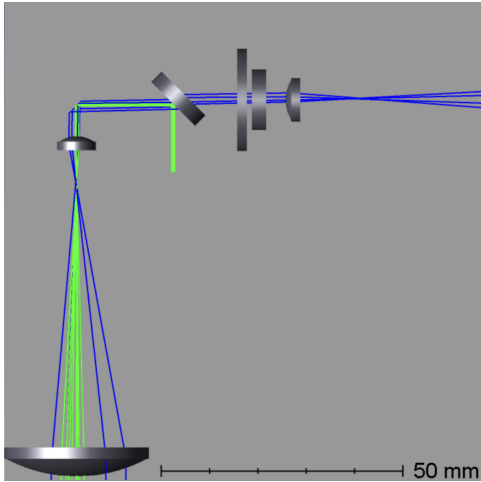


Figure 5: Zemax simulation of the entire optical assembly. FSM is represented by the beam reflection in the upper left corner, with QPD just beyond the focal point in the upper right.

### 4.2.1. Quadrant Photodiode

The currently selected QPD is an OSI Optoelectronics Q1000 InGaAs quadrant photodiode, chosen primarily for its compact form, high sensitivity, and

spectral compatibility. It provides adequate responsivity at 1064 nm, with a rise time of 0.5 ns and a noise equivalent power (NEP) of  $1.2 \times 10^{-12} \text{ W}/\sqrt{\text{Hz}}$ . It has a small active area of 1 mm.

The steering feedback loop, between the FSM and QPD, operates by digitizing the voltage distribution from the QPD and processing it with an algorithm running on the Payload controller. The controller then outputs analog voltages to actuate the fast steering mirror (FSM), steering the beam back to the QPD center and thus performing fine pointing of the transmission beam. This closed-loop pointing algorithm serves to center the OGS beacon on the QPD by producing an equal voltage distribution across all four quadrants. The algorithm itself is based roughly on those previously developed and described by Rödiger in [5], and generally works to estimate the centroid of the incident beam using the relative intensities.

To enable this, the majority of the beacon's received power must be spread over an area greater than the size of the spacing between individual quadrants (Figure 6) such that a centered beam represents a measurable, equal amount of power over each of the four quadrants. Based on the current Zemax simulation, the FWHM of the on-axis beam is approximately 0.5 mm in diameter (Figure 7). While

similar to previous design analysis [5], the team is still working on extending the simulation to derive the effective angular resolution such a beam size can offer. It may be necessary that the focal length, and thus placement of the QPD, be extended further so that the detection mechanism may have greater angular resolution.

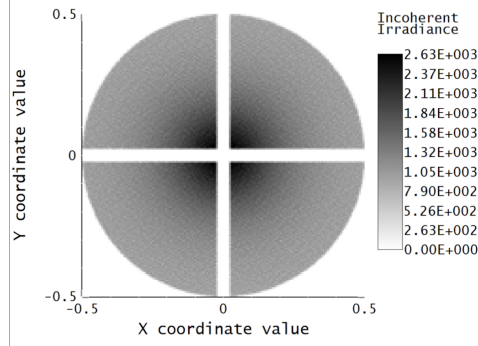


**Figure 6:** QPD power distribution (assuming approximate plane wave input at telescope aperture)

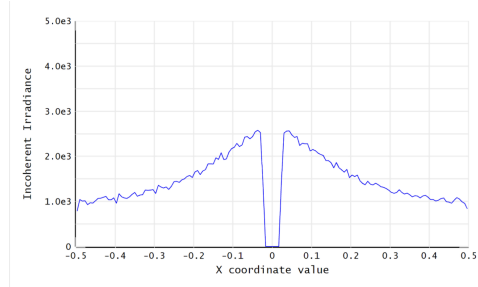


**Figure 7:** QPD power distribution near central X coordinates. The beam's power is approximately half of its maximum at +/- 0.25 mm from the QPD center.

When in use, each of the four separate QPD quadrants act as independent photodiodes, generating a reverse bias current as the Payload detects an oncoming laser from the OGS. For the current link budget, it is expected that this reverse bias current will be on the order of 9 nA and so requires significant amplification in order to be read by our Payload controller. Thus, each signal is fed into a two-stage transimpedance amplifier. The first stage performs amplification and switches the signal from a stable current to a stable voltage with a simple DC gain of  $500\text{M}\Omega$  from the feedback resistor. The second stage performs additional amplification and in the case of modulation, enacts a bandpass filter on the input. After amplification, each line is then sent through a 24-bit ADC and fed into the Payload controller.

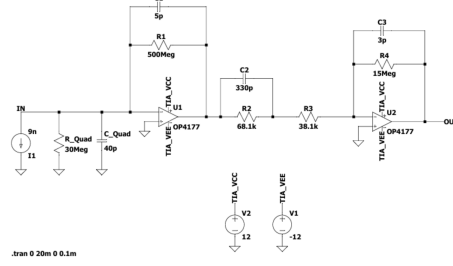


**Figure 8:** An LTspice diagram of the amplification from one quadrant of the QD. The current source represents the signal from a PD, and the OUT net is fed into an ADC.

An active priority for the team is to characterize the quadrant photodiode (QPD) spatial response by mounting it on a two-axis translation stage and focusing onto it a nanowatt-level input signal. All four quadrant outputs (Q1–Q4) are recorded on oscilloscopes with a common ground reference to establish baseline voltages. As the QPD is translated in small increments along the X and Y axes, voltage shifts are used to compute normalized beam positions and evaluate the detector's linearity and sensitivity. Future experiments will vary the beam's incidence angle—using mirrors or stage rotation—to map the QPD's angular response.

#### 4.2.2. Fine Steering Mirror

A major part of selecting the optimal FSM product depends on characterizing the performance of the FSM actuator and mirror. Thus far, the FSM performance has been characterized through Zemax simulations and data, covering the total power received and the received beam centroid on the QPD. The FSM, assuming incoming coarse-angle misalignments, will be required to tilt and to thus correct for the resulting beam misalignment from the detector. Given the current body pointing capabilities, the system requirements specify that the FSM (and other optics) must be capable of correction for at least  $1.00^\circ$  of off-axis angle of arrival. A  $1.00^\circ$  coarse-angle error with maximum FSM mechanical tilt angle is modeled using Zemax (Figure 9).

Using this model, the team found that the angle necessary for correcting the maximum mispointing was roughly  $4.1^\circ$  of tilt at the FSM, less than the target value of  $4.25^\circ$ .

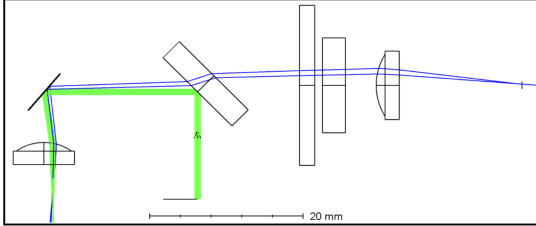


**Figure 9: 3D Optical Layout for 1.00° body pointing error with 4.25° maximum mechanical mirror tilt correction; QPD is the right-most component of the layout, blue beam representing the OGS beacon.**

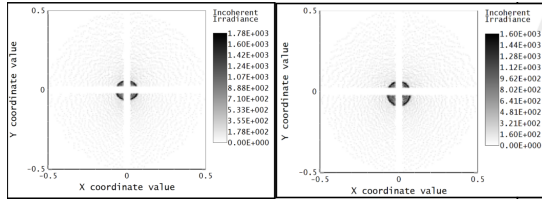


**Figure 10: Beam profile at QPD without tilting errors (Left) & QPD correction from 1.00° body mispointing using less than the 4.25° maximum mechanical mirror tilt (Right). Note that the QPD is closer to the focal plane of the focusing lens than in earlier figures, to emphasize centroid position.**

A second relevant parameter, discovered using Zemax simulations, was the effect of a tilted mirror on the beam profile that is received by the detector. Although the ground beacon body pointing misalignment is adjustable using the actuated mirror, simulated detector outputs show that greater tilts of the mirror vignette the incoming beacon beam. Effectively, the beam experiences a different on-mirror field-of-view (FOV) as the mirror's face tilts toward and away from the uplink beam's cross-sectional area. As a result of these simulations, one can obtain two major requirements on the FSM mirror (Table 3) to consider and verify with other physical testing. These requirements consider the maximum mechanical angle of the actuator, and the active diameter of the mirror.

While there are multiple methods for steering such a mirror, the Payload was generally designed around the usage of a MEMS bonded FSM, whose compact size and shape, along with limited power draw, fit the necessary requirements for the system. These mirrors, such as those commercially available from Mirrorcle Technologies, have also been used in both the O4C and CLICK-A missions. Mirrorcle Technologies offers a 4.25° maximum steering angle with a 5.00 mm bonded mirror, which will be used

for testing and verification. Of note, however, is that simulating this 5.00mm diameter mirror shows that roughly 4.79% of the uplink beacon's power misses the mirror around its edges (Figure 11). While Mirrorcle does offer a bonded, 6.4mm diameter mirror with similar maximum steering angles – which successfully receives the beacon from the telescope and reflects the entire beam to the detector (Figure 12) – the larger moment of inertia given by the increased mass and size of the mirror may negatively affect other aspects of the mirrors steering speed and vibration resistance. Thus, further testing is still necessary to determine which mirror size is most effective.

Predicted FSM Mirror Requirements from Zemax Simulations:		
Specifications:	Requirement:	Justification:
Mechanical Angle (deg.)	$\geq \sim 4.1^\circ$	Capacity for overcorrecting from 1.00° Body-Pointing Error ensures that the optimal FSM Tilt angle is within the maximum mechanical FSM Tilt range.
Active Diameter (mm)	$\geq 5.00\text{mm}$	Help to prevent vignetting along the edges of the FSM Mirror to collect the entire uplink beacon.

**Figure 11: FSM Mirror Requirements from Zemax Simulations**

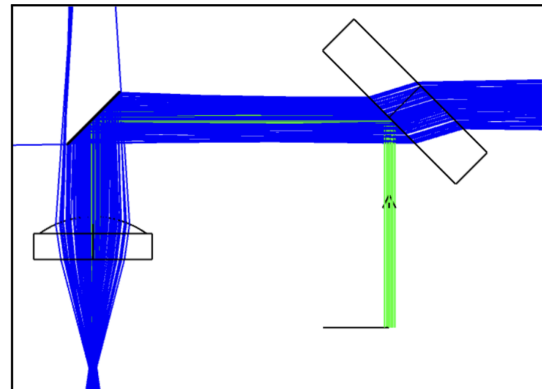


**Figure 12: The 5.0mm mirror diameter product risks imperfect collection of the ground beacon from the telescoping lenses (with 29.0mm clear entrance aperture)**

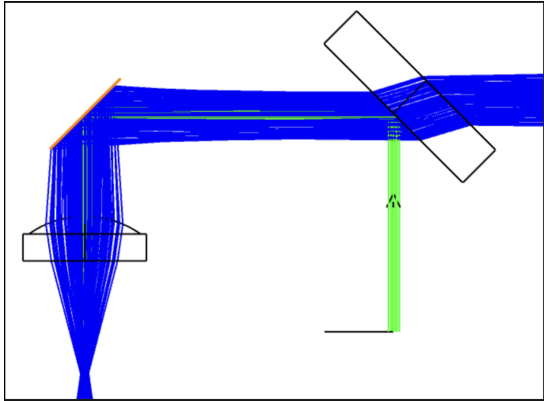


**Figure 13:** The 6.4mm mirror diameter product can collect the entire ground beacon (with 29.0mm clear entrance aperture)

Lastly, the correlation between uplink beacon angle resulting from body-pointing error, and the corresponding optimal FSM tilt that centers the beam onto the QPD is plotted in Figure 13 using simulated Zemax data. Note that the beacon angle values are zeroed around -90.00 degrees: -91.00° and -89.00° beacon tilts correspond to considering a  $\pm 1.00^\circ$  body-pointing error.

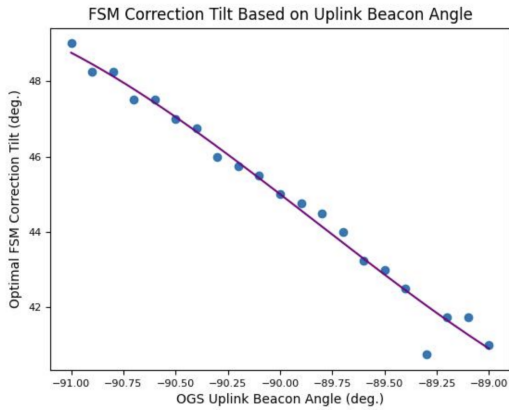


**Figure 14:** Optimal FSM Tilt adjustment required for an offset uplink beacon tilt.

#### 4.3. Transmission and Injection Assemblies

The Transmission assembly prepares a beam in two orthogonal, highly pure linear polarization states ( $DOP \geq 95\%$ ) – which is later converted to right-handed circular polarized light (RHCP) and left-handed circular polarized light (LHCP) in the Injection assembly – at 1–10 MHz modulation speed. This system was designed to meet the mission requirement for circular polarization shift key (CPolSK) data-rate and polarization purity.

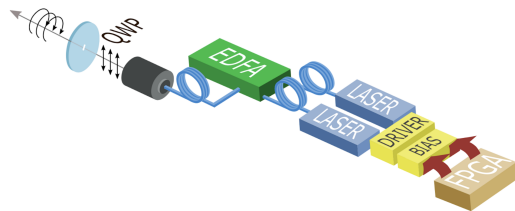


**Figure 15:** Schematic of the optical transmission path, illustrating FPGA-driven dual lasers, polarization management, and amplification prior to launching into free-space.

In the Transmission assembly, two 1550 nm wavelength stabilized polarization-maintaining (PM) fiber coupled laser diodes emit linearly polarized light along orthogonal axes, establishing the binary modulation basis for CPolSK. The binary data stream is loaded onto a Field-Programmable Gate Array (FPGA), which alternately switches the two lasers ON/OFF. Between the FPGA and the laser diodes there is a constant-current regulator that maintains diode current via onboard photodiode feedback, and a bias tee whose inductor carries the DC bias while its capacitor injects the FPGA's 10 MHz modulation onto the laser. This approach is currently being validated using our lab's LD011 driver and Thorlabs T-Bias tee, as they already meet our power, modulation-rate, and form-factor requirements, before moving to a space-qualified redesign.

A polarization-maintaining fiber combiner aligns the axes of both 1550 nm laser fiber outputs into a single PM fiber, ensuring that the orthogonal, linearly polarized beams propagate collinearly along the same optical path when emitted. This combined signal is then amplified via an EDFA, boosting the optical power from 5 mW (pre-EDFA) to 250 mW for sufficient ground detection – as link budgeting requires it. The current specification for the EDFA offers a max output of 25 dB with PM input and output (gain on both axes) and a polarization dependence of just 3-5% (which, given the architecture, will not affect the output circularity). After amplification, the beam passes through an aspheric collimator – controlling divergence for transition from fiber to free-space. A quarter-wave plate then converts each linear polarization state RHCP and LHCP.

##### 4.3.1. CPolSK Discussion

This orthogonal polarization configuration forms the basis for binary modulation in CPolSK. The modulation system encodes digital bits as distinct states of circular polarization (SOPs), with bit '1'

represented by RHCP light and bit ‘0’ by LHCP light.

An advantage to the binary data stream in the form of CPoSK is its ability to be detected regardless of variations in transmitter and receiver orientation, making it especially advantageous for dynamic scenarios, such as free-space optical links with moving platforms like the PULSE-A satellite-ground system. Since circular polarization is invariant under rotation about the propagation axis, it enables reliable data transmission without requiring polarization alignment between transmitter and receiver. In contrast with linear polarization shift keyed systems (LPolSK), which require precise coordinate alignment, CPoSK decreases the system complexity and its difficulty to operate under relative motion.

#### 4.4. Beacon Assembly

A TO-can laser diode operating at 638 nm with an output of 200 mW serves as a beacon source to aid in coarse pointing alignment between the satellite and the ground station. The designated wavelength of 638 nm was chosen due to its relatively high transmittance in clear atmospheric conditions and high responsivity for the silicon-based OGS tracking camera. This beacon provides a visible, non-data-carrying reference beam that enables the ground station to lock onto the satellite’s position.

Upon emission, the laser produces a diverging, elliptically shaped beam which passes through an aspheric collimating lens, and emerges as a parallel beam with minimal divergence. The laser diode’s collimated output exhibits an elliptical profile unless corrected by beam-shaping optics. This ellipticity reduces OGS coupling efficiency and can introduce tracking errors, as the asymmetric beam geometry limits the effective tracking area during spacecraft motion. Centroid calculations on the detector on the tracking camera must account for the beam’s elliptical profile and any dynamic changes in its orientation to ensure accurate tracking. To address this, the beam passes through a prism pair which circularizes the beam by independently adjusting the magnification along the major and minor axes of the elliptical spot. The resulting circularized and collimated 638 nm beam exits the Payload and propagates toward the OGS, where it is received. Once this alignment is achieved, the OGS can begin transmitting the 1064nm beacon to the spacecraft.

### 5. Payload Experimental Results

Payload performance is characterized through systematic testing of beam quality, pointing accuracy, and polarization integrity across operational conditions. The following section presents Payload characterization results and performance validation through preliminary component-level and system-level testing.

#### 5.1. Polarization Characterization

One of the most significant barriers to proper CPoSK data transmission is the potential alterations to the state of polarization (SOP) of the transmission laser before reaching the OGS. The Payload terminal shall preserve the transmission lasers’ linearly polarized states (LPS) before reaching the quarter-wave plate for the resulting circular polarization (RHCP or LHCP) received at the OGS to remain a well-defined and decodable signal, with minimal polarization-dependent bit errors. The most effective approach to maintain proper SOPs would be to implement a fully free-space optical terminal beginning at the laser output. However, the EDFA, which is required for signal amplification, imposes a fiber-in/fiber-out constraint. In this case, polarization-maintaining (PM) fibers are employed to preserve the LPS of the beam. They consist of a highly birefringent fiber core. They have two orthogonal axes, each corresponding to a distinct refractive index, resulting in different phase velocities for a given beam when launched into different fiber axes. This birefringent structure suppresses cross-coupling between polarization modes, enabling stable transmission of a single linear SOP over the fiber length. Thus, when an input polarization is properly aligned with either the fast or slow axis of the fiber, the SOP is maintained during the propagation and at the output.

However, transmitting light with an LPS that perfectly oscillates along one of these principal birefringent axes of the fiber proves to be difficult, as launch-induced vibrations and potential misalignment between the fiber’s principal axis and the input polarization can lead to undesirable transformations of the transmission laser’s SOP. Three primary degradation effects have been observed when a given SOP is launched misaligned with respect to a PM fiber axis: (1) depolarization ( $DOP > 100\%$ ) and its decrease) (2) introduction of a phase difference (3) polarization-dependent loss (PDL). Combined, these effects lead to the SOP at the output of the fiber, and thus what travels through the QWP at the In-

jection assembly, to be elliptically polarized, making it difficult for the OGS ground station to decode the binary information from the circular polarized light's handedness. Currently, two experiments are in progress to characterize these effects and the payload terminals' tolerance for misalignment. As shown in Figure 14, Experiment 1 was designed to simulate the linearly polarized light produced by the seed laser passing through a fiber-in/fiber-out component whose axis is not perfectly aligned with the axis of polarization. This simulation was achieved with a half-wave plate (HWP) and rotating linear polarizer (LP). The experimental setup consists of a 1550nm laser connected via PANDA PM fiber to a collimated fiber-to-fiber U-bench on which the HWP and LP were placed. The other side of the U-bench was connected, again via PANDA PM fiber, to a PAX1000VIS Polarimeter. Data was collected by rotating the LP by a given angle  $\theta$ , and by rotating the HWP by a respective  $2\theta$  to maintain alignment with the LP. By changing the degree of the axis of the polarizer and half-wave plate with respect to the fiber axis, various degrees of misalignment can be studied.

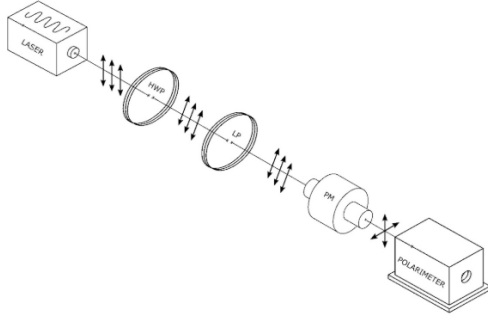


**Figure 16: Apparatus for Experiment 1.** Linearly polarized light produced by a 1550nm laser travels, via free space, through an HWP and LP before reaching a polarimeter via PM fiber.

Experiment 2, intended to model already misaligned—and thus elliptical—light passing through additional components, largely consists of the same experimental design as shown previously in Figure 14. However, an additional rotating quarter-wave plate is placed after the polarizer and HWP to turn the linearly polarized light into elliptical light (instead of a rotation of the LP axis) prior to reaching the outgoing fiber.

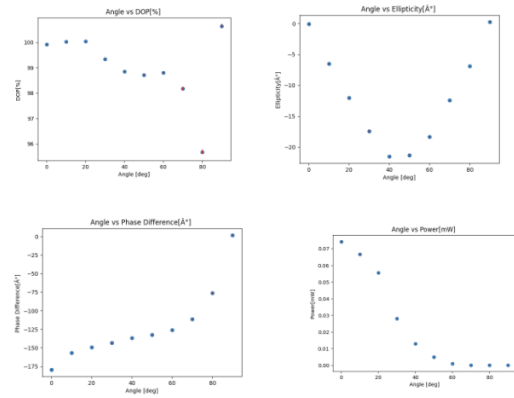


**Figure 17: Various graphs comparing the misalignment angles and properties of the propagating wave from Experiment 1 reveal how incremental increases in the misalignment between the LP/HWP and the PM-fiber axis degrade the output SOP and transmitted power.**

In experiment 1, as the misalignment angle increases from  $0^\circ$  to  $80^\circ$ , the degree of polarization (DOP) falls gradually from nearly 100% down to about 95.5%, before snapping back to 100% at a misalignment of  $90^\circ$  (i.e., when the input linear axis realigns orthogonally) (top-left). However, the first couple of degrees of misalignment consistently display a DOP close to 100%, which could indicate that if the alignment of the polarization and fiber axis is sufficiently close, DOP can be preserved.

As the misalignment angle increases, the measured ellipticity angle also begins to grow in magnitude, reaching a peak of approximately  $-22^\circ$  at  $40-50^\circ$  of misalignment. It then diminishes back toward  $0^\circ$  at a misalignment of  $90^\circ$  (top-right), indicating that the output SOP becomes highly elliptical under moderate misalignment but recovers to a linear polarization state (LPS) when the input is orthogonally aligned to the fiber axis. The phase difference between orthogonal components likewise shifts from  $-180^\circ$  toward  $0^\circ$  as the misalignment increases to  $90^\circ$  (bottom-left).

Finally, the transmitted optical power plummets from roughly 0.075 mW at perfect alignment to near zero beyond a  $70^\circ$  misalignment, before rising again at  $90^\circ$  (bottom-right), suggesting that both polarization coupling losses and misalignment critically attenuate the link. Collectively, this data confirms the necessity of maintaining the input SOP within a few degrees of the PM-fiber axis to preserve a high DOP, minimal ellipticity and sufficient power for reliable CPolSK decoding at the OGS.

To fully characterize the effects introduced by

fiber on transmission laser and its initial LPS, Mueller matrix formalism was introduced. Mueller matrices yield a method for modeling the transformation of a given SOP when propagating through an optical device such as a birefringent fiber. Given the initial and final polarization states of light propagating through an optical device, the Mueller matrix (a transformation matrix) for an optical device can be computed and used to predict the transformation of any input SOP entering this optical device. It is important to note that Mueller formalism was chosen for modeling the fiber's effect on incoming SOPs instead of Jones formalism, commonly seen in literature, because experiments point to an output of a DOP less than 100 percent, which requires Stokes vectors to fully characterize SOPs.

$$\hat{S}^t = \hat{S}^{vl} \cdot R(\theta), \quad R(\theta) = \begin{bmatrix} 1 & 0 & 0 & 0 \\ 0 & \cos(2\theta) & \sin(2\theta) & 0 \\ 0 & -\sin(2\theta) & \cos(2\theta) & 0 \\ 0 & 0 & 0 & 1 \end{bmatrix}$$

$$\hat{S}^i = R(-\theta) \cdot \hat{S}^t \cdot M^{QWP}, \quad M^{QWP} = \begin{bmatrix} 1 & 0 & 0 & 0 \\ 0 & 0 & 0 & -1 \\ 0 & 0 & 1 & 0 \\ 0 & 1 & 0 & 0 \end{bmatrix}$$

Listed are the transformations required for the Stokes vector for vertically polarized light to yield the input Stokes vectors for each SOP in experiment 2.

To fully determine the Mueller matrix (M), at least four linearly independent SOPs must be measured in terms of their Stokes parameters ( $S_0, S_1, S_2, S_3$ ); however, for improved accuracy, it is common to measure six non-degenerate SOPs (Yao et al.). Thus by measuring six non-zero, non-degenerate SOPs entering an optical device, measuring their Stokes parameters at the output, and calculating their expected input Stokes parameters via transformations, one can determine the Mueller matrix for any optical device within the Payload terminal and consequently predict any SOP output for a given SOP input into the fiber. Current work focuses on generating six well-defined (non-zero), non-degenerate states of polarization (SOPs) to enable full reconstruction of the PANDA PM fiber's Mueller matrix. Previous tests used purely linear inputs, with  $S_2 = S_3 = 0$ , which are insufficient to determine the full polarization response of the fiber. By employing a diverse set of SOPs (including elliptical and circular states), one can solve for all 16 Mueller matrix elements.

More work to establish an upper bound on allowable ellipticity for reliable OGS decoding is being done by accounting for the system's ability to perform under highly elliptical beams. This for-

malism is used to predict the final state of polarization (SOP) at the terminal output. It serves as a model for understanding how the SOP can be transformed along the optical path within the Payload. The resulting polarization transformation shall be used to inform the OGS of potential polarization-dependent bit errors during decoding. Additionally, this method can provide critical feedback to refine the payload design and justify the integration of higher-performance components, such as polarization-maintaining (PM) fiber splicing, space-hardened fiber connectors, and other precision optical interfaces, to enhance polarization stability throughout the system.

## 6. Payload Box Design

In order to meet size, weight and performance design constraints, PULSE-A's Payload uses a mechanically decoupled, multi-layer design that maintains critical optical alignment while providing standardized interfaces to the PC/104 bus. The main considerations with the Payload's design were manufacturability (can be machined with any 3-axis CNC to within  $\pm 0.13\text{mm}$ ), modularity, ease of assembly and conductance customization between layers.

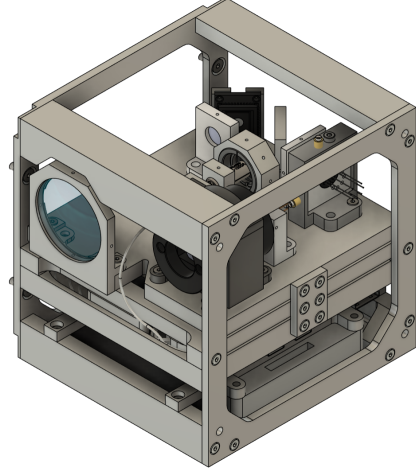


**Figure 18:** Computer-aided design of complete Payload terminal.

The payload box incorporates four parts: a structural frame, an optomechanical layer, a fiber raceway, and an amplification layer. The structural frame, machined out of Aluminum 6061, provides flexibility for choosing the placement of different layers to fit mission requirements. It is designed to interface with the bus frame on one side, and the PC/104 rails on the other, modifiable to requirements. The addition of bracket connections between

different layers allows for thermal passive control tuning through material selection. With the structural frame assembled, each layer attaches independently to facilitate testing and streamline integration. The Optomechanical layer encompasses the collimation of the downlink laser and all of the free space optics.

The fiber raceway is designed to maintain a bend radius of over 15 mm for the PM fibers, with space for splicing and connections. This layer incorporates the two seed lasers as well, with a controller on the bottom. Lastly, the amplification layer includes the EDFA, with vacant space for potential circuitry connections. Since this component generates the most amount of heat in the Payload box, it is placed on a contact face with the frame of the satellite, used for heat dissipation.

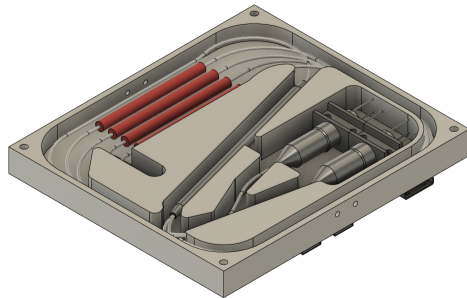


**Figure 19:** Computer-aided design of the Payload’s fiber raceway. The seed lasers are held in place by custom aluminum mounts.

### 6.1. Optomechanics

PULSE-A’s optomechanical layer was designed to be modular, with individual mounts that screw into a simple, flat breadboard. This design allows for ease of manufacturing, both because all of the parts are machineable using a 3-axis CNC, and because the design requires the optomechanical layer to be calibrated and set in-lab, reducing tolerance requirements that would otherwise be needed.

The optomechanical layer first consists of an aluminum breadboard, 6 mm thick, into which all mounts are attached. There are 9 modular mounts, each of which secures 1 Payload component, with two exceptions; the first is the quarter waveplate and the collimator, which fit into one rigid mount. The second exception is the QPD and the bandpass filter, which are mounted together in order to preserve adjustability and enable precise alignment, maintaining FSM correction accuracy.

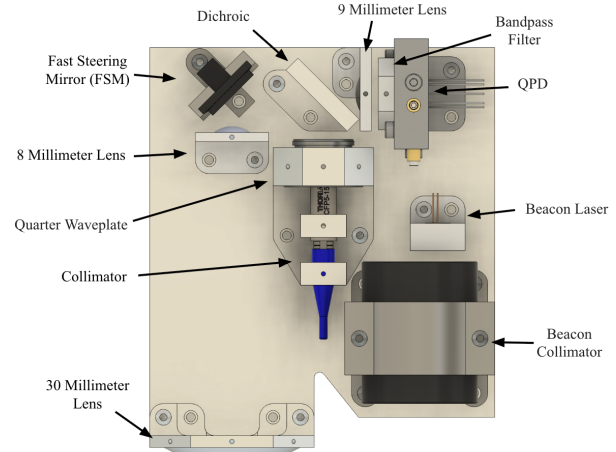


**Figure 20:** PULSE-A optical layer with labeled components.

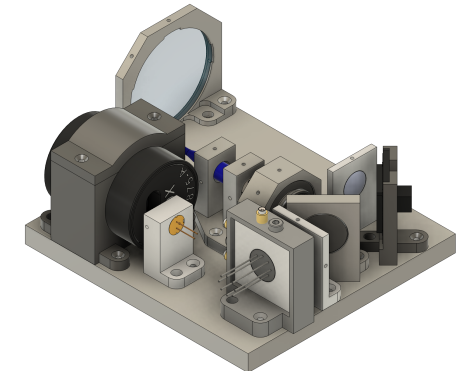


**Figure 21:** PULSE-A optical breadboard, as seen with and without the addition of optical component mounts.

To secure the optical components within the mounts themselves, RTV-566 is used, introduced through RTV injection ports situated at regular intervals around the component. Each lens mount has a protruding lip, 0.5 mm wide, which holds the lens in the correct position for epoxy.

To fix the optics into the breadboard, we use a

three-part design inspired by the CubeSat Laser Infrared CrosslinK (CLICK) team, who developed an innovative strategy for achieving high precision and stability. Our design consists of (1) a central press-fit alignment pin, 2 mm in diameter, for rigidity and alignment with the optical bench, (2) a countersunk M2 loading fastener, to further secure the mount to the breadboard, as well as provide a second point of contact to constrain rotational movement of the mount around the alignment pin. The countersunk screw head also reduces mechanical play to prevent vibration, (3) a liquid set pin, placed into the breadboard once the mount is aligned. A pin fits into a hole machined into the bench, and a slightly oversized hole in the mount above is filled with 2216 epoxy, which prevents movement due to vibration.

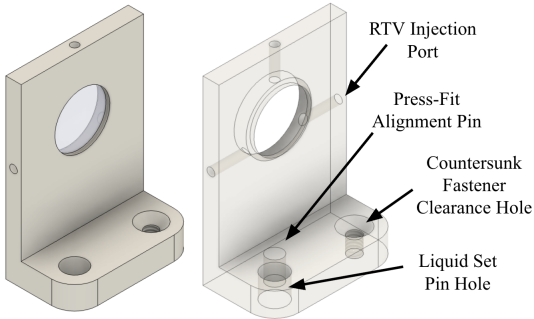


**Figure 22: PULSE-A 8 millimeter lens mount with labeled components.**

All components are fixed rigidly into the optical bench, with the exception of the QPD. The QPD is instead mounted into a support which allows for kinematic adjustment. The main base of this adjustable mount is the support mount, which is rigidly attached to the breadboard using the same press-fit alignment, countersunk bolt, and liquid set method as the other lens mounting. The QPD mount is translationally adjustable within the support mount normal to the direction of light it senses. To achieve this, bolts securing the QPD within the mount support are used in tandem with Belleville washers, which provide a preload against adjustment screws to reduce backlash and increase rigidity. The fine pitch thread on the adjustment screws allows for fine adjustments—relative to the support mount—after initial QPD positioning. The roll and translation DOF are constrained via 2 front bolts, 1 top bolt (which provides preload for 1 adjustment screw), and 1 side bolt (which provides preload for 2 adjustment screws). The base mount also holds the bandpass filter, which screws into the support via a threaded attachment. Once adjusted in-lab, the screws are also epoxied into place.

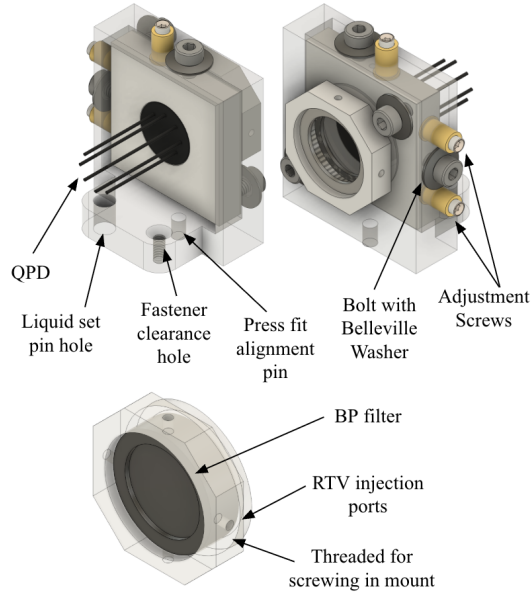


**Figure 23: PULSE-A quadrant photodiode (QPD) and bandpass filter mount and mount support with labeled components.**

## 7. Fabrication

The fabrication process began on the optomechanical layer, with the 8 millimeter lens mount, the 30 millimeter lens mount, and a baseplate for spacing. In order to reduce cost of fabrication, all CAD designs were created to be manufacturable at the on-campus machine shops, using simple 3-axis milling and CNC machines. All parts have been manufactured within a tolerance of 0.13 millimeters and were made using aluminum 6061 stock material. Preliminary collimation tests to verify Zemax lens spacings were modeled using 3D printing, with tests ultimately inconclusive due to tolerance errors associated with the FDM (Fused Deposition Modeling). Thus current and upcoming tests use machined components, and FDM is employed for assembly-plan validation (checking rough fit), and supporting hardware for lab experiments. We are currently manufacturing the payload box and the remainder of the optomechanical layer, with the intent to run preliminary vibration testing.

## 8. Further Work and Conclusions

In summary, the PULSE-A mission aims to demonstrate the feasibility of high-speed, CPolsK optical communications, challenging traditional RF systems by providing a tenfold increase in data rate

while consuming comparable power. Successful validation of PULSE-A’s system will represent a significant innovation in optical communications. In proving the viability of polarization-based modulation, PULSE-A has the potential to redefine the standard for small-sat communications, offering a scalable path to secure, high-bandwidth networks that meet the growing demand for capacity across scientific and commercial applications. PULSE-A introduces several systems for the enhancement of optical communications on the CubeSat-scale. The co-boresight beacon and transmission laser architecture, which combines the OGS beacon and CPolsK data channel, will work in tandem with the fine steering mirror of the Payload to improve pointing accuracy on the scale of sub-milliradian, beyond that guaranteed by the spacecraft’s ADCS. PULSE-A additionally intends to overcome CubeSat form factor amplification challenges, with the payload designed to preserve polarization despite the use of fiber optics. Moving forward, rigorous testing will serve to validate the terminal’s performance, with further testing including component validation, long-range pointing and accuracy, polarization integrity, link margin under expected atmospheric conditions, and data transmission characterization.

### **9. Acknowledgments**

PULSE-A’s launch is supported through the CubeSat Launch Initiative as part of NASA’s Educational Launch of Nanosatellites (ELaNa) program, notice ID #NNH23ZCF001. The project’s work is supported by the University of Chicago Pritzker School of Molecular Engineering, Department of Physics, Physical Sciences Division, Department of Astronomy and Astrophysics, as well as the Chicago Quantum Exchange. The project is further supported by the University of Chicago Women’s Board and Select Equity, LLC. We also thank our numerous private donors who supported this work.

### **References**

- [1] A. Carrasco-Casado et al., “LEO-to-ground optical communications using SOTA (Small Optical TrAnsponder) – Payload verification results and experiments on space quantum communications,” *Acta Astronautica*, vol. 139, pp. 377–384, 2017, doi: 10.1016/j.actaastro.2017.07.030.
- [2] T. Ritz, J. Conklin, D. Mayer, J. Stupl, J. Hanson, and C. Engineering, “Testing of the CubeSat Laser Infrared CrosslinK (CLICK-A) Payload,” 2020.
- [3] H. Hemmati, Ed., *Near-Earth laser communications*, Second edition. Boca Raton: CRC Press, 2021.
- [4] X. Zhao, Y. Yao, Y. Sun, and C. Liu, “Circle Polarization Shift Keying With Direct Detection for Free-Space Optical Communication,” *J. Opt. Commun. Netw.*, vol. 1, no. 4, p. 307, 2009, doi: 10.1364/JOCN.1.000307.
- [5] R. W. Kingsbury, “Optical Communications for Small Satellites,” 2015.
- [6] D. Giggenbach, M. T. Knopp, and C. Fuchs, “Link budget calculation in optical LEO satellite downlinks with on/off-keying and large signal divergence: A simplified methodology,” *Satell Commun Network*, vol. 41, no. 5, pp. 460–476, 2023, doi: 10.1002/sat.1478.
- [7] B. Rödiger et al., “High data-rate optical communication payload for CubeSats,” in *Laser Communication and Propagation through the Atmosphere and Oceans IX*, D. T. Wayne, J. A. Anguita, and J. P. Bos, Eds., Online Only, United States: SPIE, 2020, p. 3. doi: 10.1117/12.2567035.
- [8] P. Forester, “Precision Pointing for the CubeSat Laser Infrared CrosslinK (CLICK) Mission,” 2025.
- [9] A. Kaur and G. Kaur, “Polarization Shift Keying Modulation: A Novel Modulation Technique for FSO Systems,” vol. 4, no. 2, 2016.
- [10] W. Kammerer et al., “CLICK mission flight terminal optomechanical integration and testing,” in *International Conference on Space Optics — ICSO 2022*, K. Minoglou, N. Karafolas, and B. Cugny, Eds., Dubrovnik, Croatia: SPIE, 2022, p. 108. doi: 10.1117/12.2690321.